

Strain-controlled magnetic and electric polarized states in two-dimensional magnetic Janus semiconductor

Zhen Zhang,^{1,*} Jing-Yang You,^{1,*} Bo Gu,^{2,3,†} and Gang Su^{1,2,3,‡}

¹*School of Physical Sciences, University of Chinese Academy of Sciences, Beijing 100049, China*

²*Kavli Institute for Theoretical Sciences, and CAS Center for Excellence in Topological Quantum Computation, University of Chinese Academy of Sciences, Beijing 100190, China*

³*Physical Science Laboratory, Huairou National Comprehensive Science Center, Beijing 101400, China*

Two-dimensional (2D) Janus semiconductors with mirror asymmetry can introduce novel properties, such as large spin-orbit coupling (SOC) and normal piezoelectric polarization, which have attracted a great interest for their potential applications. Inspired by the recently fabricated 2D ferromagnetic (FM) semiconductor CrI_3 , the 2D Janus materials $\text{M}_2\text{Cl}_3\text{I}_3$ ($\text{M}=3d$ transition metals) are studied by the density functional theory (DFT) calculations. A stable 2D (in x-y plane) antiferromagnetic (AFM) Janus semiconductor $\text{Fe}_2\text{Cl}_3\text{I}_3$ with normal magnetization ($\mathbf{m}\parallel\mathbf{z}$) of sublattice is obtained. By applying tensile strain up to about 15%, the following four magnetic states sequentially occur: AFM with $\mathbf{m}\parallel\mathbf{z}$ of sublattice, AFM with $\mathbf{m}\parallel\mathbf{xy}$ of sublattice, FM with $\mathbf{m}\parallel\mathbf{xy}$, and FM with $\mathbf{m}\parallel\mathbf{z}$. Such novel magnetic phase diagram driven by strain can be well understood by a Heisenberg Hamiltonian with the single-ion anisotropy term, where the SOC of I atoms is found to play an essential role. In addition, the electric polarization of $\text{Fe}_2\text{Cl}_3\text{I}_3$ preserves with strain due to the broken inversion symmetry. Our results predict the Janus material $\text{Fe}_2\text{Cl}_3\text{I}_3$ as a rare example of 2D semiconductors with both spin and charge polarizations, and reveal the highly sensitive strain-controlled magnetic states and magnetization direction, which highlights the 2D magnetic Janus semiconductor as a new platform to design spintronic materials.

I. INTRODUCTION

Two-dimensional (2D) materials, such as graphene, transition metal dichalcogenides and black phosphorus [1–5], have attracted tremendous attention due to their excellent electrical, optical and acoustic properties. Although many efforts have been devoted to investigating 2D materials, the 2D semiconductors with intrinsic magnetism are still rare [6–8]. Recently, the successful synthesis of intrinsic ferromagnetic (FM) semiconductor monolayer CrI_3 [9] and bilayer CrGeTe_3 [10] with the Curie temperature of 45K and 28K, respectively, has attracted much attention on 2D magnetic semiconductors. However, potential applications of these magnets in spintronics, high Curie temperature above room temperature is highly required. In addition, the large magnetic anisotropy is needed to stabilize the magnetism in 2D systems, according to Mermin-Wagner theorem [11]. A useful approach to tune magnetism and Curie temperature is by strain [12–15], which can be realized by bending flexible substrates, elongating an elastic substrate, exploiting the thermal expansion mismatch and so on [16–22]. The band gap can also be modified by strain. For example, a transition from the direct band gap semiconductor to a metal was proposed to occur in MoS_2 monolayer with a tensile strain up to 15% [23]. The topological properties, such as the Weyl half-semimetal [24] and the room-temperature quantum anomalous Hall effect [25]

are recently proposed in the 2D ferromagnetic semiconductors. Other than FM materials, antiferromagnetic (AFM) spintronics began to take a shape, because AFM materials can not only be used as an assistant material, such as pinning layers to control the magnetization direction of the adjacent ferromagnetic layers, but also can work as a memory [26–28]. Furthermore, the spin Seebeck effect in antiferromagnets MnF_2 has recently been observed in the experiment [29]. Therefore, the investigation of the FM and AFM spintronics becomes necessary and interesting.

Among various 2D materials, the 2D Janus materials are very attractive. Compared to their prototypes, Janus materials have broken symmetries, and thus can induce many intriguing properties, such as large spin-orbit coupling (SOC), piezoelectricity, polarization, etc. [30–34]. The first graphene-based Janus material was graphene, where the Dirac cone was opened with a small gap and the FM was obtained [35]. Substituting one sulfur layer with selenium in GaS, the piezoelectric coefficient in Ga_2SSe was enhanced as large as four times [36]. The 2D Janus material MoSSe [37, 38], which has been successfully synthesized recently, not only has a better hydrogen evolution reaction efficiency, but also possesses the topological and ferroelastic properties [39] compared with its prototype MoS_2 monolayer [40].

In this work, by studying 2D Janus materials $\text{M}_2\text{Cl}_3\text{I}_3$ ($\text{M}=3d$ transition metals) on the basis of the crystal of CrI_3 , we propose a stable 2D magnetic Janus semiconductor $\text{Fe}_2\text{Cl}_3\text{I}_3$. By means of first-principle calculations, $\text{Fe}_2\text{Cl}_3\text{I}_3$ was found to be a 2D AFM semiconductor with out-of-plane magnetization ($\mathbf{m}\parallel\mathbf{z}$) of sublattice. Due to the charge redistribution caused by different electronegativity of Cl and I atoms and the broken inversion sym-

* These authors contributed equally to this work.

† gubo@ucas.ac.cn

‡ gsu@ucas.ac.cn

metry, $\text{Fe}_2\text{Cl}_3\text{I}_3$ monolayer possesses electrical polarization of about 0.18 eÅ and piezoelectricity of about 4.48 pm/V. By applying biaxial tensile strain up to about 15% on $\text{Fe}_2\text{Cl}_3\text{I}_3$ monolayer, a novel phase diagram with four magnetic states is found: AFM with out-of-plane magnetization of sublattice, AFM with in-plane magnetization of sublattice, FM with in-plane magnetization, and FM with out-of-plane magnetization. The magnetic phase can be well understood by a Heisenberg model with single-ion anisotropy term, the latter is mainly determined by the spin-orbit coupling of I atoms. Our results demonstrate a strain-controlled magnetic phases of 2D Janus magnetic semiconductors controlled by strain, and thus suggest a promising way to design functional materials.

II. COMPUTATIONAL METHODS

Our first-principles calculations were carried out with the Vienna ab initio simulation package (VASP) based on the density functional theory (DFT) [41, 42]. The interactions between nuclei and electrons were described by the projector augmented wave (PAW) method [43], and the generalized gradient approximation (GGA) in the form proposed by Perdew, Burke, and Ernzerhof (PBE) [44] was used to describe the electron exchange-correlation functional. In order to prevent the unphysical interlayer interactions, we build a 20 Å vacuum. The cut-off energy was set to be 520 eV, and the K-meshes is $9 \times 9 \times 1$ and $15 \times 15 \times 1$ G-centered Monkhorst-Pack grid [45], respectively. The structure optimization of atomic positions and the lattice vectors were done until the maximum force on each atom was less than 0.0001 eV/Å, and the total energy was converged to 10^{-8} eV. During the optimization, the conjugate gradient (CG) scheme were employed. The phonon frequencies were obtained by the density functional perturbation theory (DFPT) as implemented in the PHONOPY code [46] using a $2 \times 2 \times 1$ supercell.

III. DFT RESULTS

The crystal structure of 2D Janus $\text{Fe}_2\text{Cl}_3\text{I}_3$ is shown in Fig.1(a), where the Fe atoms are sandwiched by two different halogen atomic layers Cl and I. 2D $\text{Fe}_2\text{Cl}_3\text{I}_3$ with the broken inversion symmetry belongs to the $P31m$ (No.157) space group. Each primitive cell contains one formula units, and the Fe atoms locate in the center of the distorted octahedron consisting of three Cl atoms and three I atoms, and form a honeycomb lattice. To examine the stability of 2D $\text{Fe}_2\text{Cl}_3\text{I}_3$, its formation energy was calculated. The formation energy is defined as $E_f = E_{\text{Fe}_2\text{Cl}_3\text{I}_3} - 2E_{\text{Fe}} - 3/2E_{\text{Cl}_2} - 3/2E_{\text{I}_2}$, where $E_{\text{Fe}_2\text{Cl}_3\text{I}_3}$, E_{Fe} and E_{I_2} are energies of corresponding crystals, and E_{Cl_2} is the total energy of Cl_2 molecule.

The negative value E_f of -6.31 eV per formula unit indicates an exothermic reaction. The phonon spectra of $\text{Fe}_2\text{Cl}_3\text{I}_3$ monolayer were calculated as shown in Fig.1(c), where no imaginary frequency mode in the whole Brillouin zone indicates that $\text{Fe}_2\text{Cl}_3\text{I}_3$ monolayer is dynamically stable. The calculated lattice constant is 6.717 Å. As shown in Fig.1(d), the relative energy of $\text{Fe}_2\text{Cl}_3\text{I}_3$ as a function of applied strain changes continuously from compressed strain (-5%) to tensile strain (15%), which indicates the stability of $\text{Fe}_2\text{Cl}_3\text{I}_3$ with the applied strain.

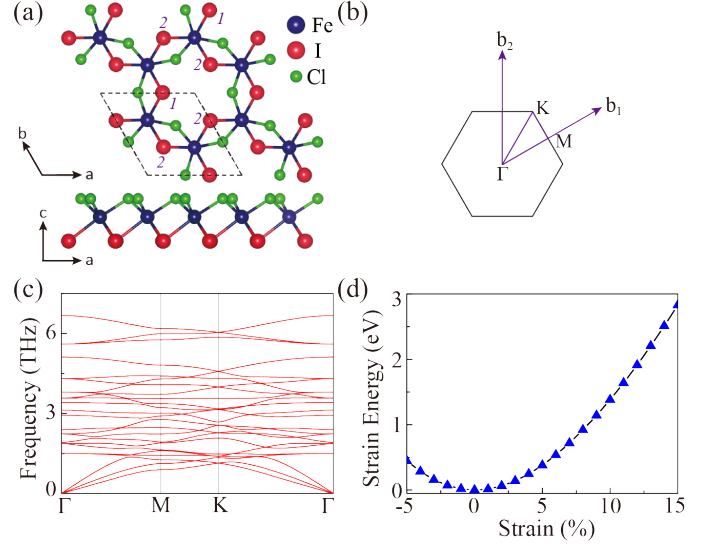


FIG. 1. (a) Top and side views of the 2D Janus material $\text{Fe}_2\text{Cl}_3\text{I}_3$ with two kinds of I atoms labeled. (b) The first Brillouin zone with high symmetry points labeled. (c) Calculated phonon spectra. (d) Strain energy as a function of applied strain.

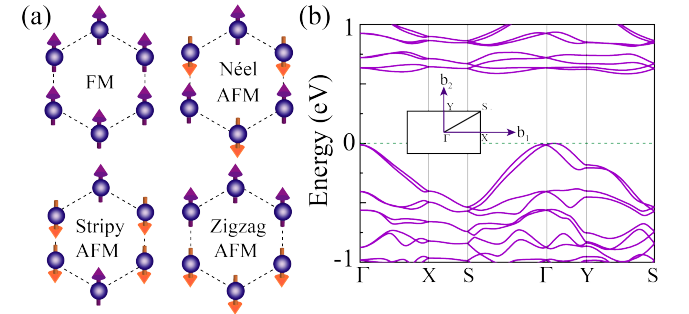


FIG. 2. (a) Possible spin configurations for Fe atoms: FM, Néel AFM, Stripy AFM and Zigzag AFM. (b) Band structure of $\text{Fe}_2\text{Cl}_3\text{I}_3$ monolayer with SOC.

The magnetic ground state of $\text{Fe}_2\text{Cl}_3\text{I}_3$ was studied by comparing the total energy of different spin configurations: FM, Néel AFM, stripy AFM, zigzag AFM and paramagnetic (PM) configurations. Table I lists the to-

TABLE I. The total energy per unit cell for $\text{Fe}_2\text{Cl}_3\text{I}_3$ monolayer (in meV, relative to the total energy of zigzag AFM along z -axis magnetization) for several spin configurations of Fe atoms calculated by GGA+SOC+U method.

Zigzag AFM($\mathbf{m} \mathbf{z}$)	Zigzag AFM($\mathbf{m} \mathbf{x}$)	Zigzag AFM($\mathbf{m} \mathbf{y}$)		
0.0	3.7	7.5		
Néel AFM($\mathbf{m} \mathbf{z}$)	Stripy AFM($\mathbf{m} \mathbf{z}$)	FM($\mathbf{m} \mathbf{z}$)	PM	
20.1	19.3	68.9	472.1	

tal energy per $\text{Fe}_2\text{Cl}_3\text{I}_3$ unit cell relative to the ground states. It is clear that the zigzag AFM with out-of-plane magnetization of sublattice possesses the lowest energy, and is the ground state. The energy difference between the ground state and the zigzag AFM with in-plane magnetization of sublattice is about 3.7 meV.

The band structure of $\text{Fe}_2\text{Cl}_3\text{I}_3$ with SOC is shown in Fig.2(b). It shows that $\text{Fe}_2\text{Cl}_3\text{I}_3$ is a semiconductor with a small indirect band gap of about 0.58 eV. Due to the different electronegativity of Cl and I atoms, the charge redistributes. According to the Bader charge analysis, one I atom gains 0.29 e from the Fe atom, and one Cl atom gains 0.55 e from the Fe atom. So a spontaneous electric polarization along the direction perpendicular to the plane with magnitude of 0.18 eÅ was obtained. Thus, the 2D Janus material $\text{Fe}_2\text{Cl}_3\text{I}_3$ is a rare example of the 2D semiconductors with both spin and charge polarizations.

The effects of biaxial strain from compress 5% to tensile 15% on the properties of 2D Janus material $\text{Fe}_2\text{Cl}_3\text{I}_3$ are explored. The MAE defined as the energy difference between the states with in-plane and out-of-plane spin configurations, ΔE defined as energy difference between the FM and AFM, and the band gap and electric polarization as a function of the strain were plotted in Fig.3. From Fig.3(a), it is noted that, ΔE decreases as the increase of tensile strain, and a phase transition from zigzag AFM to FM occurs with the tensile strain of 7%. Meanwhile, one can observe that MAE changes from positive to negative, and then returns to the positive value, corresponding to the change of magnetization direction from out-of-plane to in-plane, and then back to out-of-plane. The magnetic ground state changed with the strain can be briefly summarized as four steps: zigzag AFM with out-of-plane magnetization of sublattice, zigzag AFM with in-plane magnetization of sublattice, FM with in-plane magnetization, and FM with out-of-plane magnetization. On the other hand, the band gap and the electric polarization preserve with applied strain as shown in Fig.3(b). It is interesting to note that at tensile strain of 10%, the band gap in Fig.3(b) shows a discontinuity as a function of strain, while a magnetic phase transition occurs between FM with in-plane magnetization and FM with out-of-plane magnetization.

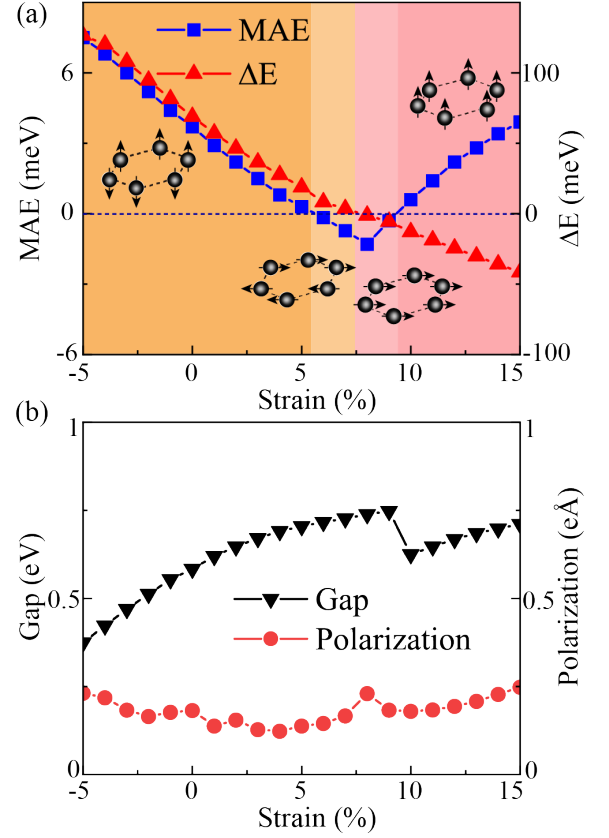


FIG. 3. Strain-dependent (a) magnetic anisotropic energy (MAE), energy difference (ΔE) between ferromagnetic and antiferromagnetic configurations and (b) band gap, electric polarization. A positive value of MAE indicates the out-of-plane magnetization, and a positive value of ΔE prefers the antiferromagnetic ground state, otherwise the opposite.

IV. MODEL ANALYSIS

To better understand the strain-controlled magnetic phase transition in $\text{Fe}_2\text{Cl}_3\text{I}_3$, the isotropic Heisenberg model including the third nearest-neighbor hoppings is employed. This model was used to explain the AFM to FM transition induced by strain in the 2D magnetic semiconductor CrSiTe_3 [47]. The model Hamiltonian can be written as

$$H_0 = \sum_{\langle i,j \rangle} J_1 \mathbf{S}_i \cdot \mathbf{S}_j + \sum_{\langle\langle i,j \rangle\rangle} J_2 \mathbf{S}_i \cdot \mathbf{S}_j + \sum_{\langle\langle\langle i,j \rangle\rangle\rangle} J_3 \mathbf{S}_i \cdot \mathbf{S}_j, \quad (1)$$

where J_1 , J_2 and J_3 represents the nearest-neighbor, next nearest-neighbor and third nearest-neighbor exchange integrals, respectively. By comparing the energies of four different magnetic configurations: FM, Néel AFM, stripy AFM and zigzag AFM, which can be expressed as a function of J_1 , J_2 and J_3 based on the classic approximation of spins in Eq. (1), the magnetic phase diagram with respect to J_1/J_2 and J_3/J_2 can be obtained as shown in Fig. 4.

On the other hand, from the DFT results of $\text{Fe}_2\text{Cl}_3\text{I}_3$ with different strains, the parameters J_1 , J_2 , and J_3 can be estimated [47, 48]. The obtained exchange parameters of $\text{Fe}_2\text{Cl}_3\text{I}_3$ are marked as stars in Fig.4, where the digital numbers of each star denote the corresponding strain.

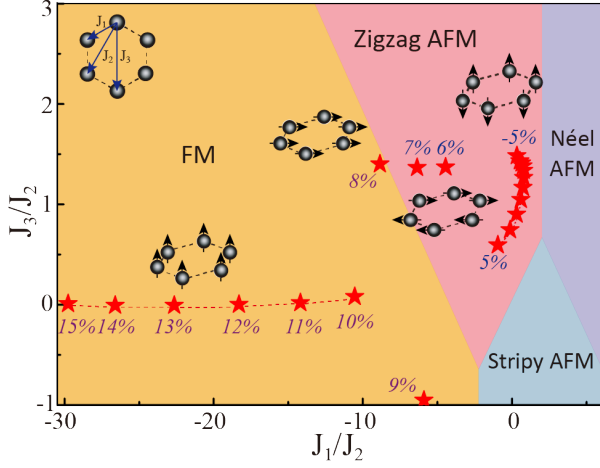


FIG. 4. Magnetic phase diagram of $\text{Fe}_2\text{Cl}_3\text{I}_3$ as a function of exchange integrals J_1/J_2 and J_3/J_2 . The DFT results with different strains are marked with stars along with the plots of the corresponding magnetic ground states.

As shown in Fig.4, $\text{Fe}_2\text{Cl}_3\text{I}_3$ locate at the zigzag AFM and FM phases. In the FM phase, the magnitude of exchange parameter J_1 is much larger than that of J_2 and J_3 , and the model Hamiltonian in Eq.(1) is simplified to the Heisenberg model with nearest-neighbor coupling J_1 . While in the zigzag AFM phase, both J_1 , J_2 and J_3 are important. Although the jump of digital numbers in the phase diagram correspond to four different magnetic ground states, the phase diagram is obtained from the isotropic Heisenberg Hamiltonian, and can't explain the change of the magnetization directions.

In order to understand the change of magnetization direction, i.e. the sign of MAE in Fig. 3(a), we consider the single-ion anisotropy (SIA), which can be written as

$$H_1 = \sum_i A_{xx} S_{i,x}^2 + A_{yy} S_{i,y}^2 + A_{zz} S_{i,z}^2, \quad (2)$$

where $A_{xx/yy/zz}$ represent the magnetic anisotropy strength of $x/y/z$ directions, $S_{i,x/y/z}$ are spin operators. According to the second-order perturbation theory, the MAE caused by SIA can be described by [49, 50]

$$E_{SIA} = \lambda^2 \sum_{o,u} \frac{|\langle \Psi_u | L_x | \Psi_o \rangle|^2 - |\langle \Psi_u | L_z | \Psi_o \rangle|^2}{\varepsilon_o - \varepsilon_u}, \quad (3)$$

where λ is the SOC constant, $L_{z/x}$ represents the angular momentum operator, Ψ_u and Ψ_o are the wavefunctions of unoccupied and occupied states, respectively, and ε_u and ε_o are the corresponding energy levels. A positive value of E_{SIA} indicates the out-of-plane magnetization, and negative value indicates the in-plane magnetization.

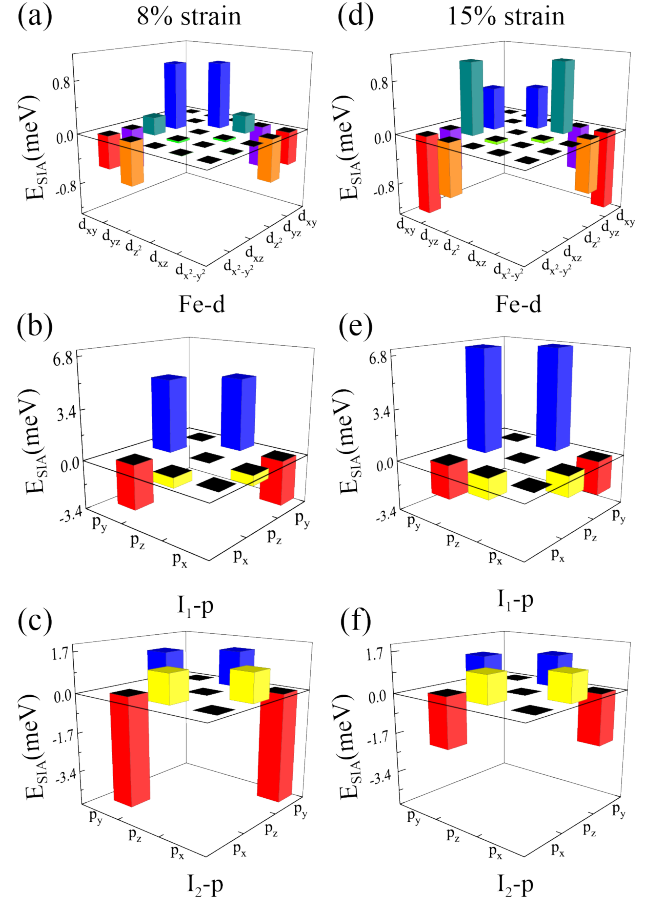


FIG. 5. Orbital-resolved single-ion anisotropy energy of Fe and two kinds of I atoms in 2D Janus $\text{Fe}_2\text{Cl}_3\text{I}_3$ monolayer with (a) 8% and (b) 15% strain. Different colors represent the contributions to E_{SIA} from different d and p orbitals of Fe and I atoms.

To unveil the mechanism that leads to the change of E_{SIA} with different strains, we have calculated the orbital-resolved E_{SIA} . As an example, the orbital-resolved E_{SIA} of $\text{Fe}_2\text{Cl}_3\text{I}_3$ with 8% and 15% tensile strains, which correspond to FM with magnetization along the x-axis and FM with magnetization along the z-axis ground states, respectively, was calculated as shown in Fig.5. By DFT calculations, the main contribution to E_{SIA} is from Fe and I atoms, and I atoms can be classified to two kinds as labeled in Fig.1(a) according to their different surroundings when the magnetization is along the x-axis. In the case of 8% tensile strain, as shown in Table II, the contributions to E_{SIA} from Fe and two kinds of I atoms are -1.2, 2.5 and -4.1 meV, respectively, giving rise to a total negative E_{SIA} of -2.8 meV. It is consistent with the in-plane magnetization. For the case of 15% tensile strain, a positive value E_{SIA} of 5.3 meV is obtained, which indicates the out-of-plane magnetization. From Fig.5, one may observe that E_{SIA} mainly originates from (p_y, p_x) , (p_y, p_z) and (p_z, p_x) matrix element of I atoms. As the tensile strain increases from 8%

TABLE II. The value of orbital-resolved single-ion anisotropy energy of Fe and two kinds of I atoms (in meV) in 2D Janus $\text{Fe}_2\text{Cl}_3\text{I}_3$ monolayer with 8% and 15% strain, respectively.

	Fe-d	I ₁ -p	I ₂ -p	Total
8%	-1.2	2.5	-4.1	-2.8
15%	-2.1	6.8	0.6	4.1

to 15%, the sign change of E_{SIA} from I atoms gives rise to the sign change of the total E_{SIA} , and thus induces the changes of the magnetization direction.

V. EFFECT OF ELECTRONIC CORRELATION

The electronic correlation effect is important for 3d orbitals in transition-metal compounds, so our above DFT calculations are carried out with $U = 4$ eV. In order to examine the influence of different U values on the magnetic ground states, we have studied the magnetic state of $\text{Fe}_2\text{Cl}_3\text{I}_3$ for the cases without strain and with 15% tensile strain with parameter U from 2 to 5 eV. As shown in Fig. 6, when there is no strain applied, with the increase of U value, although MAE increases and ΔE decreases, the signs of both preserve, indicating the unchanged AFM ground state with out-of-plane magnetization of sublattice. Similarly, the FM ground state along z-axis magnetization with 15% strain is not changed when different U values are employed. Thus, our results about the magnetic phase transition with respect to the strain are robust against U values.

VI. CONCLUSION

By first-principles calculations, we have proposed a new 2D magnetic Janus semiconductor- $\text{Fe}_2\text{Cl}_3\text{I}_3$, which was revealed to exhibit the zigzag AFM ground state with out-of-plane magnetic direction. Due to the inversion symmetry breaking and the charge redistribution, $\text{Fe}_2\text{Cl}_3\text{I}_3$ was found to possess a spontaneous polarization along the z-axis. Furthermore, we have also investigated the effect of biaxial strain on the ground state properties of $\text{Fe}_2\text{Cl}_3\text{I}_3$, and a magnetic phase transition including the antiferromagnetic-ferromagnetic transition and the change of magnetization direction was obtained. Both magnetic and electric polarization were observed in $\text{Fe}_2\text{Cl}_3\text{I}_3$ under the biaxial strain. To well understand the magnetic phase transition, a phase diagram based on the Heisenberg model with the single-ion anisotropy term can well interpret the DFT results. Our findings not only expose a new stable 2D magnetic Janus semiconductor, but also reveal the highly sensitive strain-controlled magnetic states, and thus highlight the 2D magnetic Janus

semiconductor as a new platform to design spintronic materials.

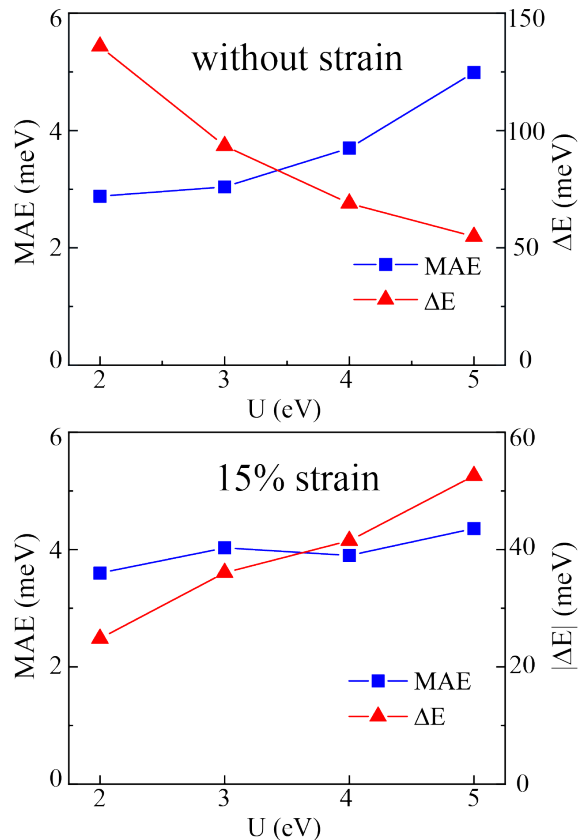


FIG. 6. Electronic correlation U -dependent magnetic anisotropic energy (MAE) and energy difference (ΔE) between antiferromagnetic and ferromagnetic configurations (a) without strain and (b) with 15% tensile strain.

VII. ACKNOWLEDGEMENTS

This work is supported in part by the National Key R&D Program of China (Grant No. 2018YFA0305800), the Strategic Priority Research Program of Chinese Academy of Sciences (Grant Nos. XDB28000000, XBD07010100), the National Natural Science Foundation of China (Grant No. 11834014), and Beijing Municipal Science and Technology Commission (Grant No. Z118100004218001). B.G. is also supported by the National Natural Science Foundation of China (Grant No. Y81Z01A1A9), the Chinese Academy of Sciences (Grant No. Y929013EA2), the University of Chinese Academy of Sciences (Grant No. 110200M208), and the Beijing Natural Science Foundation (Grant No. Z190011).

- [1] K. S. Novoselov, A. K. Geim, S. V. Morozov, D. Jiang, Y. Zhang, S. V. Dubonos, I. V. Grigorieva, A. A. Firsov, Electric field effect in atomically thin carbon films, *Science* **306**, 666 (2004).
- [2] K. S. Novoselov, D. Jiang, F. Schedin, T. J. Booth, V. V. Khotkevich, S. V. Morozov, and A. K. Geim, Two-dimensional atomic crystals, *Proc. Natl. Acad. Sci. USA* **102**, 10451 (2005).
- [3] C. Jin, F. Lin, K. Suenaga, and S. Iijima, Fabrication of a freestanding boron nitride single layer and its defect assignments, *Phys. Rev. Lett.* **102**, 195505 (2009).
- [4] K. F. Mak, C. Lee, J. Hone, J. Shan, and T. F. Heinz, Atomically Thin MoS₂: A new direct-gap semiconductor, *Phys. Rev. Lett.* **105**, 136805 (2010).
- [5] L. Li, Y. Yu, G. J. Ye, Q. Ge, X. Ou, H. Wu, D. Feng, X. H. Chen, and Y. Zhang, Black phosphorus field-effect transistors, *Nat. Nanotechnol.* **9**, 372 (2014).
- [6] M. Bonilla, S. Kolekar, Y. Ma, H. C. Diaz, V. Kalappattil, R. Das, T. Eggers, H. R. Gutierrez, M.-H. Phan, and M. Batzill, Strong room-temperature ferromagnetism in VSe₂ monolayers on van der waals substrates, *Nat. Nanotechnol.* **13**, 289 (2018).
- [7] X. Wang, K. Du, Y. Y. F. Liu, P. Hu, J. Zhang, Q. Zhang, M. H. S. Owen, X. Lu, C. K. Gan, P. Sengupta, C. Kloc, and Q. Xiong, Raman spectroscopy of atomically thin two-dimensional magnetic iron phosphorus trisulfide (FePS₃) crystals, *2D Mater.* **3**, 031009 (2016).
- [8] G. Long, T. Zhang, X. Cai, J. Hu, C. woo Cho, S. Xu, J. Shen, Z. Wu, T. Han, J. Lin, J. Wang, Y. Cai, R. Lortz, Z. Mao, and N. Wang, Isolation and characterization of few-layer manganese thiophosphite, *ACS Nano* **11**, 11330 (2017).
- [9] B. Huang, G. Clark, E. Navarro-Moratalla, D. R. Klein, R. Cheng, K. L. Seyler, D. Zhong, E. Schmidgall, M. A. McGuire, D. H. Cobden, W. Yao, D. Xiao, P. Jarillo-Herrero, and X. Xu, Layer-dependent ferromagnetism in a van der waals crystal down to the monolayer limit, *Nature* **546**, 270 (2017).
- [10] C. Gong, L. Li, Z. Li, H. Ji, A. Stern, Y. Xia, T. Cao, W. Bao, C. Wang, Y. Wang, Z. Q. Qiu, R. J. Cava, S. G. Louie, J. Xia, and X. Zhang, Discovery of intrinsic ferromagnetism in two-dimensional van der waals crystals, *Nature* **546**, 265 (2017).
- [11] N. D. Mermin and H. Wagner, Absence of ferromagnetism or antiferromagnetism in one- or two-dimensional isotropic Heisenberg models, *Phys. Rev. Lett.* **17**, 1133 (1966).
- [12] L. Webster and J.-A. Yan, Strain-tunable magnetic anisotropy in monolayer CrCl₃, CrBr₃, and CrI₃, *Phys. Rev. B* **98**, 144411 (2018).
- [13] C. Huang, J. Feng, F. Wu, D. Ahmed, B. Huang, H. Xiang, K. Deng, and E. Kan, Toward intrinsic room-temperature ferromagnetism in two-dimensional semiconductors, *J. Am. Chem. Soc.* **140**, 11519 (2018).
- [14] S. Zheng, C. Huang, T. Yu, M. Xu, S. Zhang, H. Xu, Y. Liu, E. Kan, Y. Wang, and G. Yang, High-temperature ferromagnetism in an Fe₃P monolayer with a large magnetic anisotropy, *J. Phys. Chem. Lett.* **10**, 2733 (2019).
- [15] X.-J. Dong, J.-Y. You, B. Gu, and G. Su, Strain-induced room-temperature ferromagnetic semiconductors with large anomalous hall conductivity in two-dimensional Cr₂Ge₂Se₆, *Phys. Rev. Appl.* **12**, 014020 (2019).
- [16] H. J. Conley, B. Wang, J. I. Ziegler, R. F. Haglund, S. T. Pantelides, and K. I. Bolotin, Bandgap engineering of strained monolayer and bilayer MoS₂, *Nano Lett.* **13**, 3626 (2013).
- [17] K. He, C. Poole, K. F. Mak, and J. Shan, Experimental demonstration of continuous electronic structure tuning via strain in atomically thin MoS₂, *Nano Letters* **13**, 2931 (2013).
- [18] Y. Wang, C. Cong, W. Yang, J. Shang, N. Peimyoo, Y. Chen, J. Kang, J. Wang, W. Huang, and T. Yu, Strain-induced direct-indirect bandgap transition and phonon modulation in monolayer WS₂, *Nano Res.* **8**, 2562 (2015).
- [19] Y. Y. Hui, X. Liu, W. Jie, N. Y. Chan, J. Hao, Y.-T. Hsu, L.-J. Li, W. Guo, and S. P. Lau, Exceptional tunability of band energy in a compressively strained trilayer MoS₂ sheet, *ACS Nano* **7**, 7126 (2013).
- [20] G. Plechinger, A. Castellanos-Gomez, M. Buscema, H. S. J. van der Zant, G. A. Steele, A. Kuc, T. Heine, C. Schiller, and T. Korn, Control of biaxial strain in single-layer molybdenite using local thermal expansion of the substrate, *2D Mater.* **2**, 015006 (2015).
- [21] A. Castellanos-Gomez, R. Roldán, E. Cappelluti, M. Buscema, F. Guinea, H. S. J. van der Zant, and G. A. Steele, Local strain engineering in atomically thin MoS₂, *Nano Lett.* **13**, 5361 (2013).
- [22] R. Roldán, A. Castellanos-Gomez, E. Cappelluti, and F. Guinea, Strain engineering in semiconducting two-dimensional crystals, *J. Phys.: Condens. Matter* **27**, 313201 (2015).
- [23] E. Scalise, M. Houssa, G. Pourtois, V. Afanas'ev, and A. Stesmans, Strain-induced semiconductor to metal transition in the two-dimensional honeycomb structure of MoS₂, *Nano Res.* **5**, 43 (2011).
- [24] J.-Y. You, C. Chen, Z. Zhang, X.-L. Sheng, S. A. Yang, and G. Su, Two-dimensional Weyl half-semimetal and tunable quantum anomalous Hall effect, *Phys. Rev. B* **100**, 064408 (2019).
- [25] J.-Y. You, Z. Zhang, B. Gu, and G. Su, Two-dimensional room-temperature ferromagnetic semiconductors with quantum anomalous Hall effect, *Phys. Rev. Appl.* **12**, 024063 (2019).
- [26] X. Marti, I. Fina, C. Frontera, J. Liu, P. Wadley, Q. He, R. J. Paull, J. D. Clarkson, J. Kudrnovský, I. Turek, J. Kuneš, D. Yi, J.-H. Chu, C. T. Nelson, L. You, E. Arenholz, S. Salahuddin, J. Fontcuberta, T. Jungwirth, and R. Ramesh, Room-temperature antiferromagnetic memory resistor, *Nat. Mater.* **13**, 367 (2014).
- [27] P. Wadley, B. Howells, J. elezny, C. Andrews, V. Hills, R. P. Campion, V. Novak, K. Olejnik, F. Maccherozzi, S. S. Dhesi, S. Y. Martin, T. Wagner, J. Wunderlich, F. Freimuth, Y. Mokrousov, J. Kune, J. S. Chauhan, M. J. Grzybowski, A. W. Rushforth, K. W. Edmonds, B. L. Gallagher, and T. Jungwirth, Electrical switching of an antiferromagnet, *Science* **351**, 587 (2016).
- [28] K. Olejnik, T. Seifert, Z. Kašpar, V. Novák, P. Wadley, R. P. Campion, M. Baumgartner, P. Gambardella, P. Němec, J. Wunderlich, J. Sinova, P. Kužel, M. Mller, T. Kampfrath, and T. Jungwirth, Terahertz electrical

- writing speed in an antiferromagnetic memory, *Sci. Adv.* **4**, eaar3566 (2018).
- [29] S. M. Wu, W. Zhang, A. KC, P. Borisov, J. E. Pearson, J. S. Jiang, D. Lederman, A. Hoffmann, and A. Bhattacharya, Antiferromagnetic spin seebeck effect, *Phys. Rev. Lett.* **116**, 097204 (2016).
- [30] Y. Yang, Y. Zhang, H. Ye, Z. Yu, Y. Liu, B. Su, and W. Xu, Structural and electronic properties of 2H phase janus transition metal dichalcogenide bilayers, *Superlattices Microstruct.* **131**, 8 (2019).
- [31] L. Dong, J. Lou, and V. B. Shenoy, Large in-plane and vertical piezoelectricity in Janus transition metal dichalcogenides, *ACS Nano* **11**, 8242 (2017).
- [32] Y. Guo, S. Zhou, Y. Bai, and J. Zhao, Defects and oxidation of group-III monochalcogenide monolayers, *J. Chem. Phys.* **147**, 104709 (2017).
- [33] Y. C. Cheng, Z. Y. Zhu, M. Tahir, and U. Schwingenschlögl, Spin-orbit-induced spin splittings in polar transition metal dichalcogenide monolayers, *Europhys. Lett.* **102**, 57001 (2013).
- [34] W.-J. Yin, B. Wen, G.-Z. Nie, X.-L. Wei, and L.-M. Liu, Tunable dipole and carrier mobility for a few layer Janus MoSSe structure, *J. Mater. Chem. C* **6**, 1693 (2018).
- [35] J. Zhou, Q. Wang, Q. Sun, X. S. Chen, Y. Kawazoe, and P. Jena, Ferromagnetism in semihydrogenated graphene sheet, *Nano Lett.* **9**, 3867 (2009).
- [36] Y. Guo, S. Zhou, Y. Bai, and J. Zhao, Enhanced piezoelectric effect in Janus group-III chalcogenide monolayers, *Appl. Phys. Lett.* **110**, 163102 (2017).
- [37] A.-Y. Lu, H. Zhu, J. Xiao, C.-P. Chuu, Y. Han, M.-H. Chiu, C.-C. Cheng, C.-W. Yang, K.-H. Wei, Y. Yang, Y. Wang, D. Sokaras, D. Nordlund, P. Yang, D. A. Muller, M.-Y. Chou, X. Zhang, and L.-J. Li, Janus monolayers of transition metal dichalcogenides, *Nat. Nanotechnol.* **12**, 744 (2017).
- [38] J. Zhang, S. Jia, I. Kholmanov, L. Dong, D. Er, W. Chen, H. Guo, Z. Jin, V. B. Shenoy, L. Shi, and J. Lou, Janus monolayer transition-metal dichalcogenides, *ACS Nano* **11**, 8192 (2017).
- [39] Y. Ma, L. Kou, B. Huang, Y. Dai, and T. Heine, Two-dimensional ferroelastic topological insulators in single-layer Janus transition metal dichalcogenides $\text{MSSe}(\text{M}=\text{Mo}, \text{W})$, *Phys. Rev. B* **98**, 085420 (2018).
- [40] D. Er, H. Ye, N. C. Frey, H. Kumar, J. Lou, and V. B. Shenoy, Prediction of enhanced catalytic activity for hydrogen evolution reaction in Janus transition metal dichalcogenides, *Nano Lett.* **18**, 3943 (2018).
- [41] G. Kresse and J. Hafner, Ab initio molecular dynamics for liquid metals, *Phys. Rev. B* **47**, 558 (1993).
- [42] G. Kresse and J. Furthmüller, Efficient iterative schemes for ab initio total-energy calculations using a plane-wave basis set, *Phys. Rev. B* **54**, 11169 (1996).
- [43] P. E. Blöchl, Projector augmented-wave method, *Phys. Rev. B* **50**, 17953 (1994).
- [44] J. P. Perdew, K. Burke, and M. Ernzerhof, Generalized gradient approximation made simple, *Phys. Rev. Lett.* **77**, 3865 (1996).
- [45] H. J. Monkhorst and J. D. Pack, Special points for brillouin-zone integrations, *Phys. Rev. B* **13**, 5188 (1976).
- [46] A. Togo and I. Tanaka, First principles phonon calculations in materials science, *Scr. Mater.* **108**, 1 (2015).
- [47] N. Sivadas, M. W. Daniels, R. H. Swendsen, S. Okamoto, and D. Xiao, Magnetic ground state of semiconducting transition-metal trichalcogenide monolayers, *Phys. Rev. B* **91**, 235425 (2015).
- [48] H. Xiang, C. Lee, H.-J. Koo, X. Gong, and M.-H. Whangbo, Magnetic properties and energy-mapping analysis, *Dalton Trans.* **42**, 823 (2013).
- [49] D. Sheng Wang, R. Wu, and A. J. Freeman, First-principles theory of surface magnetocrystalline anisotropy and the diatomic-pair model, *Phys. Rev. B* **47**, 14932 (1993).
- [50] B. S. Yang, J. Zhang, L. N. Jiang, W. Z. Chen, P. Tang, X.-G. Zhang, Y. Yan, and X. F. Han, Strain induced enhancement of perpendicular magnetic anisotropy in Co/graphene and Co/BN heterostructures, *Phys. Rev. B* **95**, 174424 (2017).